

# Chapter 3

## Static and Dynamic Capillarity in Silicon Based Nanochannels

Niels Tas, Nataliya Brunets, Joost W. van Honschoten<sup>†</sup>, Jeroen Haneveld, and Henri V. Jansen

**Abstract** In this chapter we review the fabrication of silicon based nanochannels and their use in capillarity studies. Static capillarity measurements of the pressure in isolated liquid plugs confined in hydrophilic nanochannels, confirm the existence of capillary negative pressure, quantitatively in accordance with the Young-Laplace equation. The negative pressure can be quantified through measurement of the elasto-capillary deformation of the channel capping due to the pressure difference with the atmospheric pressure. By measuring the capillary filling dynamics in nanochannels of uniform and accurately defined height, different (apparent) viscosity effects in confinement have been revealed. One effect (visible in insulating sub-100-nm channels) is likely to be related to the influence of the electrical double layer (an electroviscous effect), while the other effect (visible in conductive sub-50 nm channels) seems to be related to a decrease in the effective channel due to a thin immobile layer close to the polar or charged channel wall.

### 3.1 Introduction

We define capillarity as a change in the chemical potential of the liquid in a two phase system, due to the curvature of the meniscus in confinement. Capillary action plays an essential role in the retention of water in the unsaturated zone (the capillary groundwater). Related phenomena, as for example cavitation and bubble formation by enclosure of gas will have a large influence on transport in the unsaturated

---

<sup>†</sup>Deceased January 12<sup>th</sup> 2011

N. Tas (✉) • N. Brunets • J.W. van Honschoten<sup>†</sup> • J. Haneveld • H.V. Jansen  
Department of Transducers Science and Technology, MESA+ Institute for Nanotechnology,  
University of Twente, P.O. Box 217, 7500 AE Enschede, The Netherlands  
e-mail: [n.r.tas@utwente.nl](mailto:n.r.tas@utwente.nl)

zone. Silicon-based nanotechnology offers techniques for precise fabrication of artificial nano-pores. Often these channels are planar (in the plane of the substrate wafer) facilitating microscope observation of liquid inside of these channels. The combination of well-defined dimensions and observability makes silicon-based nanochannels an ideal model system for fundamental studies in capillarity. In Sect. 3.2 we will briefly review the main procedures to fabricate these nanochannels. We will then move on to discuss measurements of static capillarity in nanochannels and introduce the concept of capillary negative pressure (Sect. 3.3). Section 3.4 will be devoted to discuss experiments of dynamic capillarity, i.e. the capillary filling of nanochannels. These experiments give information on the (apparent) viscosity of water and aqueous salt solutions in confinement, a topic which is relevant to water transport in both the saturated and unsaturated zone.

### 3.2 Fabrication of Silicon Based Nanochannels<sup>1</sup>

Figure 3.1 illustrates the three main techniques for the creation of (1D-confined) nanochannels: Sacrificial layer etching (left), bulk etching (middle), and spacer layer technique (right). The sacrificial layer technique to produce nanochannels is based on the thin film encapsulation of a strip of sacrificial material and the subsequent selective removal of the sacrificial layer through access holes [1, 2] Typical combinations of materials are silicon oxide as the sacrificial layer and polysilicon as the structural material, or polysilicon as the sacrificial layer and silicon oxide or silicon nitride as the structural material. The latter combination provides optically transparent nanochannels. A practical issue in this fabrication scheme is the finite selectivity of the etchant during removal of the sacrificial layer,

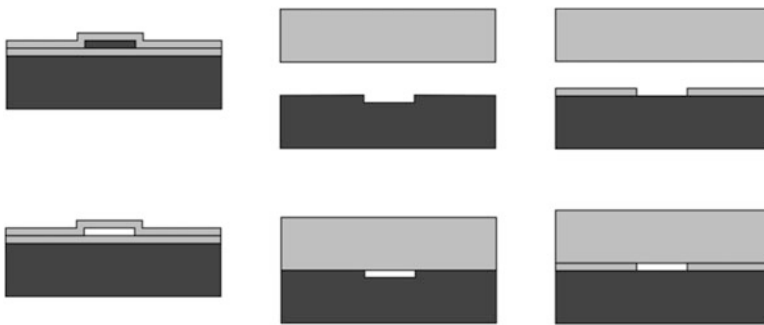


**Fig. 3.1** The three main techniques for the creation of (1D-confined) nanochannels: Sacrificial layer etching (*left*), bulk etching (*middle*), and spacer layer technique (*right*)

<sup>1</sup>This section is based on: van Honschoten JW, Brunets N, Tas NR (2012) Capillary action in silicon based nanochannels In: Ondarcuhu T, Aime JP (eds) Nanoscale liquid interfaces: wetting, patterning and force microscopy at molecular scale. Pan Stanford Publishing, Singapore.

resulting in a tapered channel height (in the length direction). In the bulk etching technique [3] a trench is slowly and accurately etched into the silicon substrate. Wet anisotropic etching can produce the required smoothness and uniformity [4]. An enclosed channel is formed by bonding of a second wafer to the substrate wafer containing the trench. This second wafer can be a glass wafer producing an optically transparent channel capping. Using wet etching [4] uniform channel heights typically in the range of 20–100 nm can be produced, with an accuracy of a few nanometer. To define the channel height for even smaller channels, the spacer layer technique [5, 6] is particularly suitable. Uniform and well defined spacer layers of silicon oxide can be created on a silicon substrate by thermal oxidation. Their thickness can be accurately measured before wafer bonding by ellipsometry, creating channels as small as 5 nm in height with a precision better than 1 nm [7]. Note that in both the bulk etching and the spacer layer technique, in practice, at least a native oxide layer of 1–2 nm silicon oxide is formed prior to wafer bonding, ensuring complete silica-based channel walls.

### 3.3 Static Capillarity in Nanochannels<sup>2</sup>

In sufficiently narrow lyophilic capillaries the negative Laplace pressure can exceed the atmospheric pressure (often 1 bar in absolute value), and a negative absolute pressure can develop in the liquid. Liquids can withstand a considerable tension due to the cohesive forces between the molecules. The tensile stress developed when the liquid is stretched is isotropic normal stress, therefore it is justified to refer to it as a negative pressure. Reports about liquids under tension date back as far as the late seventeenth and early eighteenth century, and originate from some of the greatest scientists of all time, including Huygens [8] and Newton [9]. They address the phenomenon that when a tube of a Torricelli barometer is completely filled with mercury and then perfectly purged of air and inverted, the mercury inside sometimes stayed top-full in the tube, suspended to heights as much as 75 in. [8]. This is much higher than the expected 29 inches caused by the weight of the atmosphere. In particular the explanation of Newton is remarkably accurate, referring to the cohesion of the liquid particles to each other and to the glass composing the tube [9]. Tension in water plays a central role in the cohesion-tension theory of sap ascent in trees as first proposed by Dixon and Joly [10], and has therefore drawn the interest of plant physiologists. Classical laboratory methods to induce negative pressures in liquids are the Berthelot tube method [11] based on isochoric cooling, and the rotating capillary technique introduced by Briggs [12].

Bulk liquid at negative absolute pressure is superheated, which is a metastable state. It is a metastable state because the system can move to a state of lower free energy by creating cavities filled by vapour, however to create a cavity (vapour bubble) an energy barrier has to be overcome [13]. If the liquid is at a pressure

---

<sup>2</sup>This section is based on: van Honschoten JW, Brunets N, Tas NR (2010) Chem Soc Rev 39: 1096.

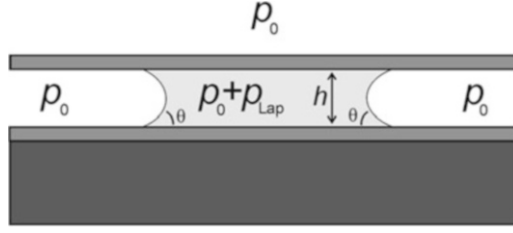


**Fig. 3.2** Longitudinal section of a partially filled flat rectangular capillary. The pressure in the liquid is equal to the ambient pressure  $p_0$  plus the negative Laplace pressure  $p_{Lap}$ . The channel height is  $h$  the contact angle of the liquid to the channel walls is represented by  $\theta$

$p$ , then the work required to create a bubble of volume  $V$  and surface area  $A$ , filled with vapour at a pressure  $p_v$  is given by [13]:

$$W = \gamma A + (p - p_v) V = 4\pi r^2 \gamma + \frac{4}{3} \pi r^3 (p - p_v) \quad (3.1)$$

where  $r$  is the radius of the bubble, and  $\gamma$  is the surface tension of the liquid. Assuming that the magnitude of  $p$  is much larger than  $p_v$ , the work required to create the bubble has a maximum  $16\pi\gamma^3/3p^2$  for a critical radius [13]:

$$r_{crit} = -2\gamma/p \quad (3.2)$$

The capillary action in narrow lyophilic tubes, in open communication with the surrounding atmosphere, can easily be stronger in magnitude than the surrounding absolute atmospheric pressure. Figure 3.2 shows a longitudinal section of such a capillary, partially filled with liquid. The absolute pressure in the liquid is given by the sum of the ambient pressure  $p_0$  and the negative Laplace pressure  $p_{Lap}$ .

Assume in Fig. 3.2 that we have a thin rectangular capillary (height  $h \ll$  width). Neglecting the meniscus curvature in the lateral plane, the pressure of the liquid phase  $p_{liq}$  is given by:

$$p_{liq} = p_0 - (2\gamma \cos \theta) / h \quad (3.3)$$

where  $h$  is the channel height,  $\gamma$  the surface tension of the liquid, and  $\theta$  the contact angle of the liquid to the channel walls. If the liquid partially filling the hydrophilic channel is water, capillarity induced negative pressure will occur when the channel height is below approximately  $1 \mu\text{m}$ . The first notion that capillary action in narrow tubes can induce tension in the liquid was probably by Kelvin when he derived what is now known as the Kelvin equation [14]. Experimental proof of the existence of capillary negative pressure was provided by Wiig and Juhola [15] through the measurement of a reduced density of water condensed in nano-porous activated charcoal, though quantitative interpretation was hampered by the unknown compressibility of water in the negative pressure regime as well as lack of exact knowledge of the pore diameter.

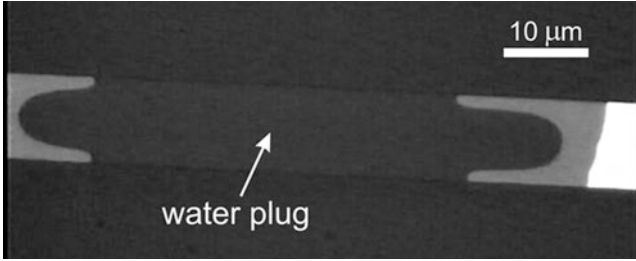


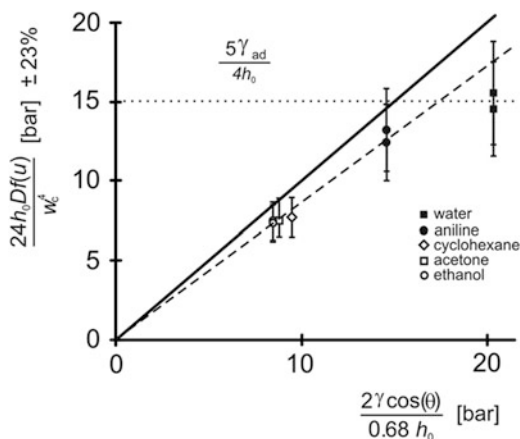
**Fig. 3.3** Top view of a silicon oxide nanochannel (flat rectangular cross section) partially filled by water [17]. The channel capping is a silicon oxide thin film which deforms under the negative pressure load. This deformation can explain the peculiar shape of the meniscus [17, 18]

Through pull-off force measurements in a surface forces apparatus [16] consistency with Young-Laplace equation could be confirmed in nanometric gaps, however in this method the conversion from forces to pressures requires application of the Kelvin equation. A direct indication for the existence of capillary negative pressures was recently found by measuring the elasto-capillary deformation of silicon based nanochannels [17]. Figure 3.3 shows a microscope image of the typical shape of the meniscus (top view of a flat rectangular channel). The peculiar curvature of the meniscus in the lateral plane can be explained by a downward bending of the flexible channel cover. The downward bending can be quantified by detailed analysis of the meniscus shape [17, 18]. Together with the known stiffness of the channel cover it was possible to estimate the negative pressure of the liquid to be, depending on the method to analyse the meniscus curvature,  $-17 \pm 10$  bar [17] or  $-14 \pm 8$  bar [18]. Taking into account the measurement accuracy, this is in accordance with Eq. (3.3) ( $-12$  bar).

Liquid plugs like the one shown in Fig. 3.3 are remarkable stable and can (depending on their volume and the speed of evaporation) exist for several minutes up to hours. The explanation for this observation [17] is that when we substitute Eq. (3.3) in the expression for the critical bubble size (Eq. (3.2)) we find (neglecting  $p_0$  with respect to the negative Laplace pressure)  $r_{crit} = h/\cos(\theta)$ . This shows that for capillary negative pressure the critical bubble size for cavitation is larger than the size of the channel, so the liquid at negative pressure is in a stable state. Note also that we have implicitly considered channels of uniform cross section.

A related technique to measure capillary negative pressure is to look at the critical width of total collapse for nanochannels capped by an elastic cover plate [19]. Using this technique we measured capillary negative pressure in 80 nm channels for different liquids (as a function of their surface tension). Figure 3.4 shows the measured mechanical deformation pressure needed for total collapse (vertical) as a function of the applied capillary pressure (horizontal). Although limited in accuracy these results are indicative for the validity of the Young-Laplace equation in the sub-100 nm regime.

**Fig. 3.4** Measured and expected mechanical deformation pressure versus the capillary pressure [19]. The expected relation is indicated by the *solid line* with slope one, the *dashed line* indicates the trend line in the experimental data. Where  $h_0$  is the initial channel height,  $Df(u)$  an elasticity parameter, and  $w_c$  is the critical width for full collapse [19]



### 3.4 Dynamic Capillarity in Nanochannels<sup>3</sup>

This section addresses the dynamics of filling of capillaries of arbitrary, though uniform cross section, typically in the 10–100 nm size range. For simple liquids at this length scale the continuum framework of hydrodynamics based on application of the Navier-Stokes equations is still valid, as is discussed in detail in the review by Bocquet and Charlaix [20]. Also the macroscopic contact angle and Young-Laplace equation can be applied without modifications. For smaller cross sections (hydrodynamic diameters less than roughly 10 nm) the influence of the disjoining pressure on the microscopic contact angle and the meniscus curvature can be become noticeable (in particular for water where the electrostatic contribution to the disjoining pressures can be relative long ranging) and care should be taken by applying the macroscopic Young and Young-Laplace equations. The systematic study of capillary filling of sub-10 nm channels is still in its infancy and will most likely be subject of study of several groups in upcoming years.

#### 3.4.1 Lucas-Washburn Equation for Infinite Stiff Channels

The filling dynamics of capillaries driven by the negative Laplace pressure was first modeled by Washburn [21]. The filling speed is determined by the surface tension  $\gamma$  of the liquid filling the capillary, its (advancing) contact angle  $\theta$  to the channel walls, the channel diameter  $d$  (or in the case of a rectangular cross section by the width  $w$  and the height  $h$ ) and finally by the viscosity  $\eta$  of the liquid. For sufficiently long and narrow capillaries the flow of the liquid entering the capillary may be

<sup>3</sup>This section is based on: van Honschoten JW, Brunets N, Tas NR (2010) Chem Soc Rev 39: 1096.

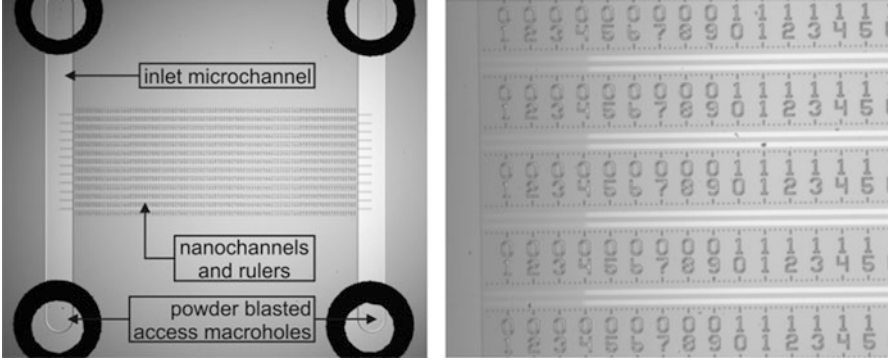


**Fig. 3.5** Top view of a chip (appr.  $1 \times 1 \text{ cm}^2$ ) used in capillary filling experiments (left) [23]. Zoom in showing a still image of the filling of 30 nm channels (right) [7]

considered laminar and fully developed and the hydraulic resistance  $R = (\text{pressure drop } \Delta p)/(\text{volume flow } \phi)$  follows from the Poiseuille flow model. Taking the negative of the Laplace pressure for the pressure drop and realizing that the change of the position  $x$  of the moving meniscus is related to the volume flow through  $dx/dt = \phi/A$  (where  $A$  is the cross sectional area of the channel) the following general expression for the position of the moving meniscus as a function of time results:

$$x dx = \frac{-p_{Lap}}{R^* \cdot A} dt \quad (3.4)$$

where  $R^*$  is the hydraulic resistance per unit length of the liquid plug ( $R = xR^*$ ). As the hydraulic resistance is proportional to the liquid plug length  $x$ , it follows that the filling velocity decreases in time. More precisely, after integration the result is  $x^2 \sim t$  or  $x \sim t^{1/2}$ . For example for a flat rectangular channel ( $w \gg h$ ) by substitution of  $R^*$  and  $p_{Lap}$  we find:

$$x = \sqrt{\frac{\gamma \cos(\theta) h}{3\eta} \cdot t} \quad (3.5)$$

In recent years this expression has been experimentally verified in silicon based nanochannels with a perfectly defined rectangular cross section, and down to channel heights of 5 nm [6, 7, 22–25] the qualitative  $x = at^{1/2}$  dependence has been confirmed for water and aqueous solutions as well as for some organic liquids. Figure 3.5 shows a photograph of a chip used in such experiments. Liquid can be introduced in the access holes and fills the chip by capillary action, first through the inlet microchannel, then through the nanochannels. Rulers have been etched next to the nanochannels to follow the filling process in time.

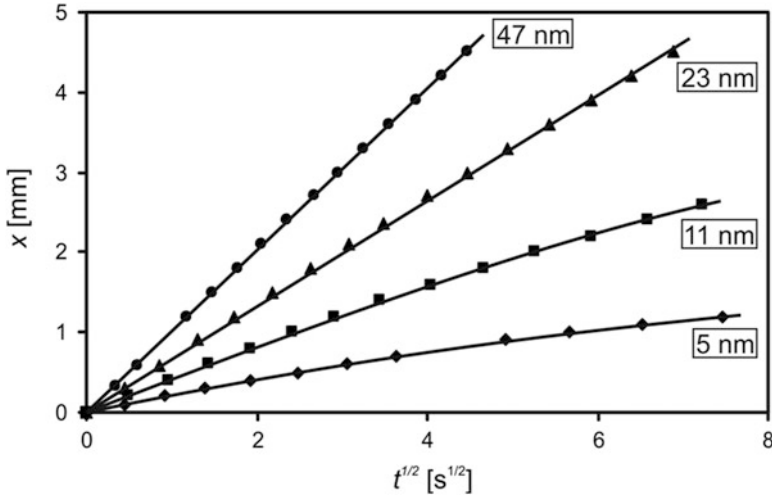


**Fig. 3.6** Measured position of the moving meniscus as a function of  $t^{1/2}$  for filling of 5, 11, 23, and 47 nm deep nanochannels with DI water at temperatures of 22.7, 22.2, 21.6, and  $20.8 \pm 0.5$  °C, respectively [7]

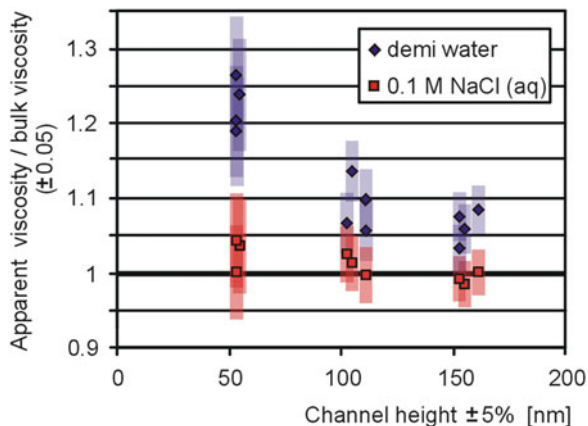
### 3.4.2 Results of Capillary Filling Experiments in Nanochannels

Figure 3.6 shows an example of the measured position of the moving meniscus vs. time in capillary filling of hydrophilic nanochannels by de-ionized water (silicon-dioxide channel bottom and boro-silicate glass channel roof, rectangular cross section  $h \ll w$ ). Note that down to the level of  $h = 5$  nm the moving meniscus can be observed by optical microscopy, for the smallest channel heights using differential interference contrast (DIC) [7] or an embedded interferometer [25] to enhance the contrast. In the analysis of the filling dynamics usually macroscopic contact angles and surface tension values are used, which for small molecules should be correct when channel hydraulic diameters are in the order of 10 nm or more.

While the qualitative agreement with the Washburn model is good, several significant quantitative deviations have been observed. As they all concern slower than expected filling they are usually described by a dimensionless apparent viscosity  $\eta_{app}/\eta$  larger than 1 (where  $\eta_{app}/\eta = 1$  refers to the situation described by Eq. (3.5)). Figure 3.7 shows the results as reported by Tas et al. [23] for filling of silica channels (20 nm SiO<sub>2</sub>, borosilicate glass channel cover), by de-ionized water (DI water) and aqueous 0.1 M NaCl solution. A significant slower than expected filling for DI-water was attributed to the electroviscous effect, as the values of  $\eta_{app}/\eta$  returned to one when filling the channels by aqueous NaCl solutions. The electroviscous effect is related to the electrical double layer that is formed when the capillary walls in contact with the liquid are charged (see Schoch et al. [26])



**Fig. 3.7** Ratio of the apparent viscosity over the bulk viscosity of de-ionized water (*blue*) and aqueous NaCl solution (*red*) as derived from capillary filling experiments [23]



for an extensive review of electrokinetic effects in nanochannels). Due to the flow a net displacement of charge and an induced streaming potential results, which results into a counter electro-osmotic flow in a part of the electrical double layer that is closest to the channel walls [27]. A comparison [28] of the observed value of  $\eta_{app}/\eta$  with the theory of Levine, however, is not easy because of deprotonation of the hydroxylated channel walls during filling [29], leading to a modified and possibly axially non-uniform ionic composition of the solution filling the channels. In addition, it is likely that the constant potential assumption should be replaced by some form of charge regulation.

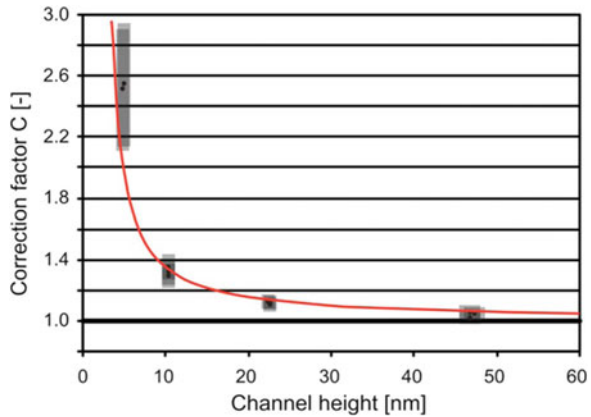
An important aspect of capillary filling, especially in channels having sharp inner corners, is the formation of bubbles [30]. In sharp inner corners a strong capillary suction develops, which leads to capillary “fingers” possibly proceeding in front of the main meniscus. The length of these fingers depends on the filling time and the “consumption” at the back by the proceeding main meniscus. As the main meniscus slows down in time the length and volume of the fingers tends to increase and eventually can lead to bubble formation through enclosure of air in front of the main meniscus. It has been suggested [30] that the presence of bubbles can be responsible for the sometimes observed slower than expected filling as shown in Fig. 3.7. However, the Washburn model is derived for filling without bubbles and should therefore only be applied to the length where the first bubbles are formed [23].

### 3.4.3 The Viscosity of Water in nm-Confinement

Since the early 1970s there is a notion that water near polar or charged surfaces is somehow ordered or structured, leading to a so called structural component of the disjoining pressure. The first indications came from interpretation of the disjoining pressure isotherms of wetting films of water on hydrophilic substrates

[31], while unambiguous experimental proof came through application of the so called Surface Forces Apparatus (SFA) [32–36] showing short range repulsion forces between charged surfaces brought in close proximity ( $< 5$  nm), in addition to the double layer repulsion and van der Waals attraction as described by the DLVO theory. Despite the enormous importance of water as a liquid in nature as well as engineering systems, the exact nature of this hydration force as it is called for water has still not been conclusively determined. The main mechanisms that have been discussed in literature are related to the compression of hydrated ions (ionic surface groups, adsorbed ions, or counter-ions in the electrical double layer), orientation of water dipoles in the strong electric field near a charged wall, or the hydrogen bonding nature of water. An important question that emerges is if and how the supposed interfacial “structuring” of water affects its local viscosity. In the early 1970s measurements of the flow velocity of liquid plugs in quartz microcapillaries driven by a disbalance between the capillary pressure and an applied external pressure revealed an elevated viscosity of water up to 40 % in capillaries of  $0.04 \mu\text{m}$  [37]. These results could not be reproduced in nanometer thin films in the SFA. A dynamic SFA technique revealed a viscosity of water equal to the bulk viscosity, even in 2 nm thin films and under high salt concentrations necessary to induce a strong repulsive hydration force between the mica surfaces [38]. A similar conclusion was reached by SFA squeeze out experiments of thin water films between silica surfaces [36]. More recently, in a SFA where also shear force can be induced and measured, Raviv et al. [39] found that the viscosity of demineralized water when confined to films of  $3.5 \pm 1$  to  $0.0 \pm 0.4$  nm between mica surfaces remains within a factor three of its bulk value. Similar experiments with aqueous salt solution (in the presence of repulsive hydration forces) show that the bounded water molecules in the hydration layers retain the shear fluidity characteristics of bulk water, with an upper limit estimated for the viscosity of  $0.08 \text{ Pa} \cdot \text{s}$  (maximum of 80 times the bulk viscosity) [40]. Remarkably, recent AFM experiments, measuring directly and simultaneously the normal and lateral forces of a nano-sized silicon tip approach a solid hydrophilic surface, reveals orders of magnitude increase in the viscosity of water with respect to bulk water in sub-nanometer confinement [41]. Capillary filling of silica nanochannels by water and aqueous salt solutions, reveals a significant slower than expected filling in channels with heights in the range of 10–50 nm [6, 7]. If interpreted as a viscosity effect, the averaged effective viscosity is up 30 % higher for 11 nm channels [7] (Fig. 3.8). The red line is a fit to the experimental data assuming a highly viscous layer next to the hydrophilic channel walls. The best fit is found for a thickness of this immobile layer of 0.9 nm at each interface. Filling experiments under different conditions are currently carried out in our lab to test the hypothesis that it is indeed the enhanced viscosity of hydration layers that causes the observed slower than expected filling. Based on all experimental data available, one must conclude that the question if and how hydration forces are connected to viscosity changes of interfacial water has still not been completely answered.

**Fig. 3.8** Dimensionless correction factor (pre-factor of the denominator in Eq. (3.5)) indicating a slower than expected filling of water in flat rectangular silica nanochannels [7], as a function of channel height. The red line indicates the effect of a solidified layer next to the channel walls with a thickness of 0.9 nm or four monolayers



### 3.5 Conclusions

Planar silicon based nanochannels offer a unique platform for experimental studies of capillarity in extreme confinement. In many cases processes inside the nanochannels can be observed by standard optical microscopy. In lyophilic nanochannels the extreme confinement can easily lead to large negative pressures in the liquid. These can be measured by quantifying the elastic deformation of the channels. Dynamic capillarity studies using water or aqueous salt solutions revealed an increased apparent viscosity during capillary filling of nanochannels. The increased apparent viscosity is attributed to an electroviscous effect in the case of insulating channels. For channels well below 50 nm there is an additional effect leading to a strong increase of the apparent viscosity. It is unclear if this is a real increase in the viscosity of water strongly confined in hydrophilic channels. Alternatively, it could be caused by the combination of the properties of water and immobile adsorbed ions.

### References

1. Stern MB, Geis MW, Curtin JE (1997) Nanochannel fabrication for chemical sensors. *J Vac Sci Technol B* 15:2887–2891
2. Turner SW, Perez AM, Lopez A, Craighead HG (1998) Monolithic nanofluid sieving structures for DNA manipulation. *J Vac Sci Technol B* 16:3835–3840
3. Han J, Craighead HG (1999) Entropic trapping and sieving of long DNA molecules in a nanofluidic channel. *J Vac Sci Technol A* 17:2142–2147
4. Haneveld J, Jansen H, Berenschot E, Tas N, Elwenspoek M (2003) Wet anisotropic etching for fluidic 1D nanochannels. *J Micromech Microeng* 13:S62–S66
5. Haneveld J (2006) Nanochannel fabrication and characterization using bond micromachining. Ph.D. Thesis, University of Twente

6. Persson F, Thamdrup LH, Mikkelsen MBL, Jaarlgard SE, Skafto-Pedersen P, Bruus H, Kristensen A (2007) Double thermal oxidation scheme for the fabrication of SiO<sub>2</sub> nanochannels. *Nanotechnology* 18(245301):1–4
7. Haneveld J, Tas NR, Brunets N, Jansen HV, Elwenspoek M (2008) Capillary filling of sub-10 nm nanochannels. *J Appl Phys* 104(014309):1–6
8. Huygens C (1672) An extract of a letter of M. Hugens to the author of the *Journal des Scavans* of July 25. 1672. Attempting to render the cause of that odd phenomenon of the quicksilver remaining suspended far above the usual height in Torricellian experiment. *Philos Trans* 7:5027–5030
9. Sir Isaac Newton (1721) *Opticks: or a treatise of the reflections, refraction, inflections and colours of light*, 3rd Book, 3rd edn, pp 365–366
10. Dixon HH, Joly J (1895) On the ascent of sap. *Philos Trans R Soc Lond B* 186:563–576
11. Berthelot M (1850) Sur quelques phénomènes de dilatation forcée des liquides. *Annales de chimie et de Physique* 30:232–237
12. Briggs LJ (1950) Limiting negative pressure of water. *J Appl Phys* 21:721–722
13. Fisher JC (1948) The fracture of liquids. *J Appl Phys* 19:1062–1067
14. Kelvin L (1870) On the equilibrium vapour at a curved surface of liquid. *Proc R Soc Edinb* 7:63–68
15. Wiig EO, Juhola AJ (1949) The adsorption of water vapor on activated charcoal. *J Am Chem Soc* 71:561–568
16. Fisher LR, Israelachvili JN (1980) Determination of the capillary pressure in menisci of molecular dimensions. *Chem Phys Lett* 76:325–328
17. Tas NR, Mela P, Kramer T, Berenschot JW, van den Berg A (2003) Capillarity induced negative pressure of water plugs in nanochannels. *Nano Lett* 3:1537–1540
18. van Honschoten JW, Escalante M, Tas NR, Elwenspoek M (2009) Formation of liquid menisci in flexible nanochannels. *J Colloid Interface Sci* 329:133–139
19. Tas NR, Escalante M, van Honschoten JW, Jansen HV, Elwenspoek M (2010) Capillary negative pressure measured by nanochannel collapse. *Langmuir* 26:1473–1476
20. Bocquet L, Charlaix E (2010) Nanofluidics, from bulk to interfaces. *Chem Soc Rev* 39:1073–1095
21. Washburn EW (1921) The dynamics of capillary flow. *Phys Rev* 17:273–283
22. Hibara A, Saito T, Kim H-B, Tokeshi M, Ooi T, Nakao M, Kitamori T (2002) Nanochannels on a fused-silica microchip and liquid properties investigated by time-resolved fluorescence measurements. *Anal Chem* 74:6170–6176
23. Tas NR, Haneveld J, Jansen HV, Elwenspoek M, van den Berg A (2004) Capillary filling speed of water in nanochannels. *Appl Phys Lett* 85:3274–3276
24. Han A, Mondin G, Hegelbach NG, de Rooij NF, Stauer U (2006) Filling kinetics of liquids in nanochannels as narrow as 27 nm by capillary force. *J Colloid Interface Sci* 293:151–157
25. van Delft KM, Eijkel JCT, Mijatovic D, Druzhinina TS, Rathgen H, Tas NR, van den Berg A, Mugele F (2007) Micromachined Fabry-Perot interferometer with embedded nanochannels for nanoscale fluid dynamics. *Nano Lett* 7:345–350
26. Schoch RB, Han J, Renaud P (2008) Transport phenomena in nanofluidics. *Rev Mod Phys* 80:839–883
27. Levine S, Marriotti JR, Robinson K (1975) Theory of Electrokinetic flow in a narrow parallel-plate channel. *J Chem Soc Faraday Trans* 2(71):1–11
28. Mortensen NA, Kristensen A (2008) Electroviscous effects in capillary filling of nanochannels. *Appl Phys Lett* 92(063110):1–3
29. Jansen KGH, Hoang HT, Floris J, de Vries J, Tas NR, Eijkel JCT, Hankemeier T (2008) *Anal Chem* 80:8095–8101
30. Thamdrup LH, Persson F, Bruus H, Kristensen A, Flyvbjerg H (2007) Experimental investigation of bubble formation during capillary filling of SiO<sub>2</sub> nanoslits. *Appl Phys Lett* 91(163505):1–3
31. Derjaguin BV, Churaev NV (1974) Structural component of disjoining pressure. *J Colloid Interface Sci* 49:249–255

32. Israelachvili JN, Adams GE (1978) Measurement of forces between two mica surfaces in aqueous electrolyte solutions in the range 0–100 nm. *J Chem Soc Faraday Trans* 74:975–1001
33. Pashley RM (1981) Hydration forces between mica surfaces in aqueous electrolyte solutions. *J Colloid Interface Sci* 80:153–162
34. Pashley RM (1981) DLVO and hydration forces between mica surfaces in  $\text{Li}^+$ ,  $\text{Na}^+$ ,  $\text{K}^+$  and  $\text{Cs}^+$  electrolyte solutions: a correlation of double-layer and hydration forces with surface cation exchange properties. *J Colloid Interface Sci* 83:531–546
35. Pashley RM, Israelachvili JN (1984) Molecular layering of water in thin films between mica surfaces and its relation to hydration forces. *J Colloid Interface Sci* 101:511–523
36. Horn RG, Smith DT, Haller W (1989) Surface forces and viscosity of water measured between silica sheets. *Chem Phys Lett* 162:404–408
37. Churaev NV, Sobolev VD, Zorin ZM (1971) Special discussion in thin liquid films and boundary layers. Academic, New York, pp 213–220
38. Israelachvili JN (1986) Measurement of the viscosity of liquids in very thin films. *J Colloid Interface Sci* 110:263–271
39. Raviv U, Lurat P, Klein J (2001) Fluidity of water confined to subnanometre films. *Nature* 413:51–54
40. Raviv U, Klein J (2002) Fluidity of bound hydration layers. *Science* 297:1540–1543
41. Li T-D, Gao J, Szoszkiewicz R, Landman U, Riedo E (2007) Structures and viscous water in subnanometer gaps. *Phys Rev B* 75(115415):1–5